Journal of Molecular Graphics and Modelling 27 (2008) 286–298

Contents lists available at ScienceDirect

Journal of Molecular Graphics and Modelling

journal homepage: www.elsevier.com/locate/JMGM

Structural basis for ligand recognition at the benzodiazepine binding site of $GABA_A$ α3 receptor, and pharmacophore-based virtual screening approach

R.S.K. Vijayan, Nanda Ghoshal *

Structural Biology and Bioinformatics Division, Indian Institute of Chemical Biology, 4 Raja S.C. Mullick Road, Jadavpur, Kolkata 700032, India

ARTICLE INFO

Article history:
Received 18 March 2008
Received in revised form 29 April 2008
Accepted 5 May 2008
Available online 9 May 2008

Keywords:
Benzodiazepine receptor
3D QSAR
Pharmacophore modeling (HipHop)
Scaffold hopping
Message–Address concept

ABSTRACT

Given the heterogeneity of $GABA_A$ receptor, the pharmacological significance of identifying subtype selective modulators is increasingly being recognized. Thus, drugs selective for $GABA_A$ α_3 receptors are expected to display fewer side effects than the drugs presently in clinical use. Hence we carried out 3D QSAR (three-dimensional quantitative structure–activity relationship) studies on a series of novel $GABA_A$ α_3 subtype selective modulators to gain more insight into subtype affinity. To identify the 3D functional attributes required for subtype selectivity, a chemical feature-based pharmacophore, primarily based on selective ligands representing diverse structural classes was generated. The obtained pseudo receptor model of the benzodiazepine binding site revealed a binding mode akin to "Message–Address" concept. Scaffold hopping was carried out across multi-conformational May Bridge database for the identification of novel chemotypes. Further a focused data reduction approach was employed to choose a subset of enriched compounds based on "Drug likeness" and "Similarity-based" methods. These results taken together could provide impetus for rational design and optimization of more selective and high affinity leads with a potential to have decreased adverse effects.

1. Introduction

γ-Amino butyric acid (GABA), the principal inhibitory neurotransmitter in the mammalian central nervous system exerts its physiological effects by binding to three major classes of receptors, namely $GABA_A$, $GABA_B$ and $GABA_C$ [1]. The $GABA_A$ receptor, along with nicotinic acetylcholine receptor (nAChR), glycine receptor (GlyR) and 5-hydroxytryptamine (5-HT3) receptor, belongs to Cys-loop super family of ligand-gated ion channels (LGIC) [2]. Of all these ion channels $GABA_A$ receptor has received the greatest attention in terms of research because of its importance as a biological target for clinically important drugs like barbiturates, neurosteroids, loreclezole, anesthetics, ethanol, and benzodiazepines (BDZs) [3,4]. The $GABA_A$ receptor is a membrane bound hetero pentameric complex arranged pseudo symmetrically around a central Cl^- selective ion channel [5]. Purification, cloning and sequencing of the $GABA_A$ receptor and its composite subunits have allowed identifying 21 subunits arranged within 8 families (α1–6, β1–4, γ1–4, 1δ, 1ε, 1π, 1θ and ρ1–3) [6]. Although in principle these subunits can combine to form a large number of $GABA_A$ receptors, current in vivo studies evidence only 13 functional subtype combinations [6]. The proposed stoichiometry of the three subunits in the pentamer is 2α, 2β, 1γ [5]. Currently used Benzodiazepines, the most commonly prescribed class of psychoactive drugs in current medical practice, are nonselective agonists and are associated with side effects such as amnesia, tolerance, dependence and alcohol potentiation. Recent studies have shown that ligands with functional selectivity for $GABA_A$ α_2 and α_3 receptor subtypes act as non-sedating anxiolytics in animal models [7–9].

As computational tools have become an integral part of drug discovery, we undertook a comprehensive molecular modeling study to identify the pertinent features that could serve as a starting point for design of ligands with increased affinity and target selectivity. In this context, 3D QSAR (three-dimensional quantitative structure–activity relationship) receptor mapping techniques, such as, molecular field analysis (MFA) and receptor surface analysis (RSA) were used to construct an atomistic picture of hitherto unsolved receptor site that would be constructive in identifying molecular features that account for affinity. Since increased affinity to a particular receptor subtype does not guarantee for increased selectivity with respect to a given receptor subtype, a second strategy was embarked to generate a ligand-based pharmacophore model aimed at identifying pertinent features conferring selectivity. The obtained pharmacophore

* Corresponding author. Tel.: +91 33 2473 3491x254; fax: +91 33 2473 0284/5197.
E-mail address: nghoshal@iicb.res.in (N. Ghoshal).

1093-3263/$ – see front matter © 2008 Elsevier Inc. All rights reserved.
doi:10.1016/j.jmgm.2008.05.003

model was validated for its enrichment ability. Scaffold hopping was performed using pharmacophore-based queries across multi conformational compound database followed by the creation of a focused subset, using various computational filters.

2. Experimental methodology

All molecular modeling calculations outlined herein were performed on Silicon Graphics Fuel workstation running on IRIX 6.5 operating system. The software packages used in the present study were Cerius^2 Version 4.10 [10], Catalyst Version 11 [11], CS Chem Draw Ultra 6.0 [12] and SPSS Version 12.0.1 [13].

2.1. Data set modeling

Data set compounds were modeled using the 3D Sketcher module of Cerius^2. Partial atomic charges were assigned using the Gasteiger method. Initial geometries of the molecules were optimized using energy optimization cycles. Conformational ensemble scanning was performed using annealing dynamics, with user defined attributes—req. temp. −450 K, dynamics time step −0.01 ps, steps 10,000, using constant number of moles, volume and energy (NVE). Annealing dynamics was followed by energy minimization. The used force field was UNIVERSAL 1.02 and the molecules were minimized to high convergence on the smart minimizer using 500 iterations or more if required [14].

2.2. Biological data and K-means cluster analysis (K-MCA)-based series design

An internally consistent data set in terms of activity range, distribution, assay method and experimental conditions were taken from a single literature source reported by Russel et al. [15]. The skewness in the dataset was removed by converting K_i values to pK_i. A non-hierarchical method called *K*-means clustering was performed using SPSS for the rational division of a training and test series. Manual selection of compounds was done from each cluster so as to ensure that the training set and test set had adequate coverage in terms of activity range and 'chemical diversity' [16]. Accordingly 63 compounds were used for training and the rest 13 compounds served as test set.

The data set used for the generation of QSAR by MFA and RSA are shown in Table 1, and their core scaffolds are shown in Fig. 1(A)–(C).

Table 1
Training and test sets compounds with observed and predicted pK_i values

Compound	R group	Observed pK_i	G/PLS predicted (MFA)	G/PLS predicted (RSA)
1	4-MeO-Ph	7.283	7.214	7.476
2	2-Me-Ph	6.552	6.932	6.637
3	3-Me-Ph	6.853	6.947	6.748
4	4-Me-Ph	7.494	7.222	7.279
5	2-F-Ph	8.214	7.725	7.844
6	4-F-Ph	7.236	6.919	7.293
7	4-Pyridyl	7.886	7.725	7.760
8	3-Me-2-pyridyl	8.677	8.406	7.730
9	4-Me-2-pyridyl	7.744	7.845	7.760
10	5-Me-2-pyridyl	7.828	7.511	7.705
11	6-Me-2-pyridyl	7.698	7.914	7.738
12	3-Pr-2-pyridyl	8.619	8.641	8.516
13	3,6-DiMe-2-pyridyl	8.443	8.735	8.596
14	3,5-DiMe-2-pyridyl	9.148	8.733	8.591
15	3,4-DiMe-2-pyridyl	8.769	8.729	8.575
16	3-MeO_2C-2-pyridyl	8.148	8.250	8.585
17	3-HO-2-pyridyl	6.744	7.517	7.361
18	3-MeO-2-pyridyl	8.619	8.730	8.252
19	3-EtO-2-pyridyl	8.958	8.734	8.630
20	3-Cyclopropyl-methoxy-2-pyridyl	8.638	8.572	8.631
21	3-BnO-2-pyridyl	7.698	7.878	8.220
22	Pyridazin-3-yl	8.070	7.649	7.744
23	Pyrimidin-4-yl	8.508	8.267	7.814
24	Pyrazin-2-yl	8.522	8.714	8.371
25	6-Me-pyridazin-3-yl	8.000	7.507	7.383
26	6-Cl-pyridazin-3-yl	7.638	7.626	7.815
27	Isoquinolin-1-yl 29	8.346	8.183	8.047
28	Quinoxalin-2-yl	7.585	7.156	7.085
29	2-Pyridylethoxy	6.698	6.734	7.364
30	1-(2-Pyridyl)ethoxy	6.259	6.523	6.639
31	2-CN-$PhCH_2O$	7.275	7.724	7.657
32	3-CN-$PhCH_2O$	7.180	6.911	7.616
33	3-$HOCH_2$-$PhCH_2O$	7.366	7.599	7.814
34	4-$HOCH_2$-$PhCH_2O$	7.356	7.632	7.156
35	3-Me_2NCH_2-$PhCH_2O$	7.619	8.087	7.176
36	4-MeSO-$PhCH_2O$	7.508	7.606	7.004
37	1-Me-piperidin-3-ylmethoxy	6.337	6.300	6.470
38	5-Oxo-2-pyrrolidinemethoxy	6.585	6.913	7.630
39	Me_2NCOCH_2O	7.050	6.930	6.650
40	1-Pyrrolidine-$COCH_2O$	7.301	7.495	7.517
41	BnMeN$COCH_2O$	7.387	7.588	7.693
42	Hydroxypropoxy	6.769	6.937	6.951
43	Hydroxybutoxy	7.721	7.203	7.705
44	Pyrazol-1-yl	7.721	8.273	7.814
45	3,5-DiMe-pyrazol-1-yl	8.638	8.265	8.629
46	Imidazol-2-yl	8.173	8.054	8.333

Table 1 (*Continued*)

Compound	R group	Observed pK_i	G/PLS predicted (MFA)	G/PLS predicted (RSA)
47	1-Me-imidazol-2-yl	8.366	8.150	7.914
48	4-Me-imidazol-2-yl	8.107	7.630	7.780
49	1-Et-imidazol-2-yl	9.000	8.799	9.091
50	1-Bn-imidazol-2-yl	8.698	8.794	8.708
51	5-Me-isoxazol-3-yl	7.744	7.848	7.731
52	4-Me-thiazol-2-yl	7.522	7.487	7.260
53	5-Me-thiazol-2-yl	7.619	7.881	7.758
54	5-Me-thiazol-4-yl	7.920	8.269	8.051
55	Benzothiazol-2-yl	6.602	6.894	6.553
56	3-Me-isothiazol-5-yl	7.000	6.897	7.706
57	3-Me-1,2,4-oxadiazol-5-yl	7.292	7.384	7.793
58	5-Me-1,2,4-oxadiazol-3-yl	7.180	7.384	7.767
59	1,2,4-Triazol-3-yl	7.721	7.505	7.761
60	1-Me-1,2,4-triazol-3-yl	8.096	7.729	7.732
61	2-Me-1,2,4-triazol-3-yl	8.552	8.230	8.384
62	1-Pr-1,2,4-triazol-3-yl	7.397	7.841	7.765
63	1-Me-tetrazol-5-yl	7.677	8.074	7.745
Test set				
64	Ph	7.886	7.393	7.814
65	3-MeO-Ph	7.537	7.222	7.264
66	3-Pyridyl	7.602	7.627	7.362
67	3-CN-2-pyridyl	8.769	8.734	8.314
68	3-Methoxyethoxy-2-pyridyl	8.408	8.148	8.380
69	Pyrimidin-2-yl	7.481	7.639	7.321
70	Quinolin-2-yl	7.113	7.236	7.102
71	6-Me-2-pyridylpropoxy	6.619	7.167	7.275
72	4-CN-PhCH_2O	7.154	6.912	7.538
73	Thiazol-2-yl	7.721	7.728	7.768
74	Thiazol-4-yl	8.000	8.142	7.376
75	2-Pr-1,2,4-triazol-3-yl	8.853	8.759	8.490
76	2-Me-tetrazol-5-yl	7.431	7.392	7.719

2.3. Structure alignment for 3D QSAR

The dataset compounds were aligned in space using the core substructure search (CSS) alignment keeping the align strategy as consensus. This superposition assumes that the aligned molecules share a common global shape and location in the 3D lattice, hence entropic contributions to free energy are expected to be similar [17]. The aligned geometry of the compounds is shown in Fig. 2.

2.4. 3D QSAR (MFA and RSA) methodology

Molecular field analysis (MFA) is a 3D QSAR technique implemented in Cerius^2, similar to CoMFA (comparative molecular field analysis). Three different probes, CH_3, H^+, and HO^- were used to simulate steric, electrostatic and hydrogen bonding interactions, respectively. Energies outside the range of +30 to −30 kcal were truncated. A reduced grid spacing of 2.0 Å was used so as to decrease the noise in *X* variables and hence to obtain a statistically significant model [17].

Energies associated with each of the MFA grid points were calculated and variable reduction was performed choosing only 10% of those information rich descriptors with highest variance. All variables were normalized and the length of the final equation was set to 12 terms. Genetic partial least squares (G/PLS) derived from the best features of two methods, genetic algorithm (GA) and partial least squares (PLS), was used for feature selection and fitting [18,19]. The best model was obtained on a population size of 100 with 25,000 generations. The mutation probabilities were kept at system default. The G/PLS model derived was optimal with four components as determined by q^2 (cross-validated square correlation coefficient). A variable usage graph displayed during each G/PLS run was used to monitor premature convergence of GA.

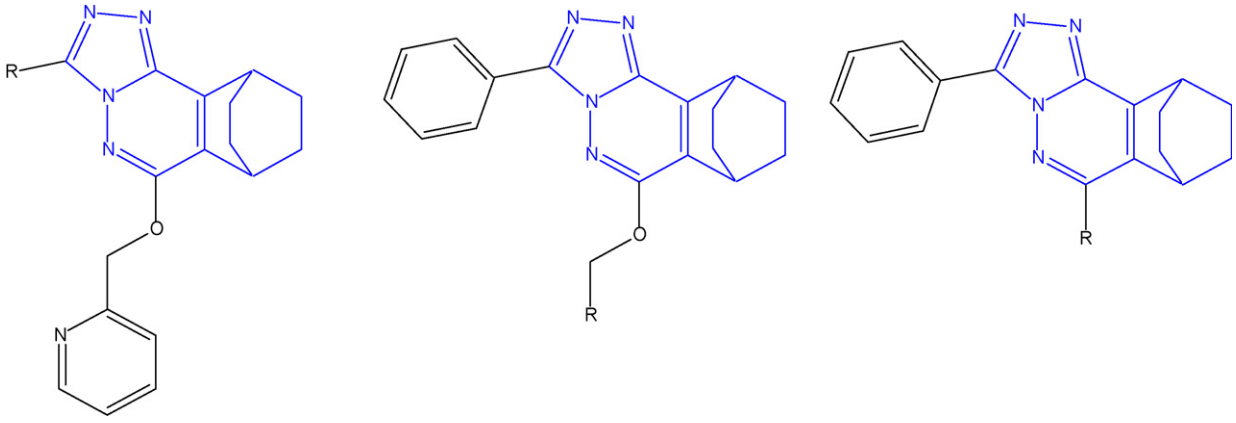

Fig. 1. The core scaffolds (A–C) of pthalazine derivatives used in the data set. (A) Compounds **1**–**6** and **64**, **65**. (B) Compounds **7**–**41** and **66**–**74**. (C) Compounds **42**–**56** and **75**, **76**. Common core scaffold used for alignment is shown in blue.

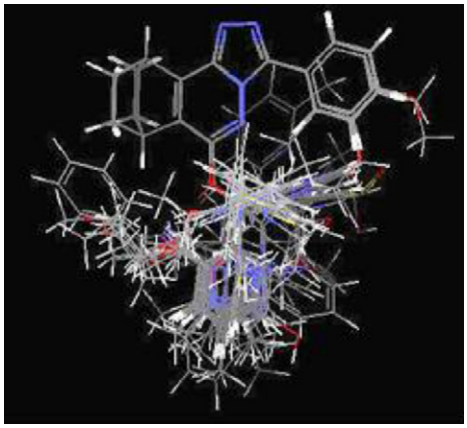

Fig. 2. A view of the aligned geometry of all compounds used for MFA and RSA studies.

Another atomistic psuedo receptor modeling technique termed receptor surface modeling (RSM) was performed on the same set of aligned molecules. RSM differs from grid-based approaches like CoMFA, MFA and GRID and is more chemically relevant, because it exists on a surface that is shaped like a molecule. The receptor surface was generated, using van der Waals field function, with weights proportional to biological activity. Various properties namely charge, electrostatic potential, hydrogen bonding propensity and hydrophobicity associated with every 25 *N*th surface point was evaluated and used as *X* variable in a quantitative fashion for receptor surface analysis (RSA).

RSA analysis was carried out using G/PLS method consisting of 5000 crossover generations on a population of 100 parent equations. The equation length was set to 10 terms including a constant. Both linear and non-linear terms were used. Regression using spline terms allows the incorporation of non-linear modeling [20]. G/PLS model obtained for RSA was optimal with five components as determined by q^2.

2.5. Ligand-based pharmacophore model

To probe the 3D functional attributes implicated in selectivity, a feature-based 3D pharmacophore model that represents the pharmacophoric requirements, deemed responsible for selectivity, was mapped from a set of highly selective ligands. The most promising model thus obtained could be used as 3D queries to search for new structural leads across publicly available multi conformational databases. To ensure structural diversity among the data set, 13 non-congeneric molecules known to exhibit functional selectivity were chosen as structural templates from literatures [15,21–29].

The 2D structures of the compounds, used for the generation of pharmacophore, are summarized in Fig. 3. Catalyst HipHop algorithm, which identifies common chemical features from a set of ligands without the use of affinity data [30] was used. This approach sounds plausible when compounds are pooled from different literature sources. Conformation coverage was sampled for each molecule using the Poling algorithm [31]. The "best conformer generation" option, with maximum number of conformers set to 250 with an energy range of 20 kcal/mol, was used for conformer generation. In generating the hypothesis, chemical features were selected from the feature dictionary. In a receptor guided approach, one can consider features that are directly involved in ligand binding. Since we followed a ligand-based approach, the feature definitions were defined so as to cover all the facets of ligand–receptor interactions. The feature definitions considered for the generation of the pharmacophore were hydrogen bond acceptor (HBA), hydrogen bond acceptor (HBA lipid), hydrogen bond donor (HBD), hydrophobic, hydrophobic aliphatic, hydrophobic aromatic and ring aromatic. Catalyst was forced to find a model with HBA lipid and hydrophobic aliphatic, since these two features were common in all actives. The permitted inter feature spacing was set to 1 Å. Since all the compounds in question were known to be selective, we had no reasons to prefer one compound to other, hence all the molecules were considered as reference (principal = 2, max omit feat = 0). Maximum likelihood criterion was used to rate the hypothesis [30]. Quantitative estimation of the goodness of match between a molecule and the pharmacophore was estimated using the (Fit) option and the values are reported as fit values in Fig. 3.

2.6. Pharmacophore-based virtual screening

The pharmacophore model developed using HipHop was used as a query for virtual screening (VS). For this purpose we used a refined "Target specific pharmacophore" that defines the functional and steric requirements for selective ligand binding. The hits obtained were further enriched using Lipinski's rule of five [30] (Filter 1) and PCA (principal component analysis)-based similarity clustering (Filter 2) [30].

3. Results and discussion

3.1. 3D QSAR (MFA and RSA) analysis

The major objective while working with MFA analysis was to find the best predictive model with the used dataset, hence many equations were generated for the same data set using various parameters and the best MFA model obtained in terms of statistical significance is expressed as

$$\begin{aligned} \mathrm{p}K_i = {} & 7.90103 - 0.020786 \times \text{“H}^+/716\text{”} - 0.017094 \times \text{“HO}^-/708\text{”} \\ & +0.011199 \times \text{“H}^+/484\text{”} + 0.014201 \times \text{“H}^+/404\text{”} - 0.019656 \times \text{“HO}^-/486\text{”} \\ & +0.021768 \times \text{“CH}_3/314\text{”} + 0.018701 \times \text{“H}^+/397\text{”} + 0.018734 \times \text{“CH}_3/484\text{”} \\ & -0.016121 \times \text{“HO}^-/585\text{”} - 0.0221 \times \text{“CH}_3/419\text{”} + 0.024579 \times \text{“CH}_3/326\text{”} \end{aligned} \quad (1)$$

$N_{\text{Training}} = 63$, $N_{\text{Test}} = 13$, optimal number of components (ONC) = 4,
$R^2 = 0.821$, adjusted R^2 (R^2_{adj}) = 0.808, Bs $R^2 = 0.798$, R^2_{cv} (q^2) = 0.814,
randomized $R^2 = 0.462$, SDEP = 0.300, LSE = 0.086, PRESS = 5.784,
$R^2_{\text{Pred}} = 0.833$, standard error of estimate (S) = 0.307, $\text{AVRES}_{\text{Test}} = 0.037$,
$\text{RMSE}_{\text{Test}} = 0.254$, $S_{\text{PRESS}} = 0.315$, $(R^2 - R^2_0)/R^2 = 0$, $k = 1$

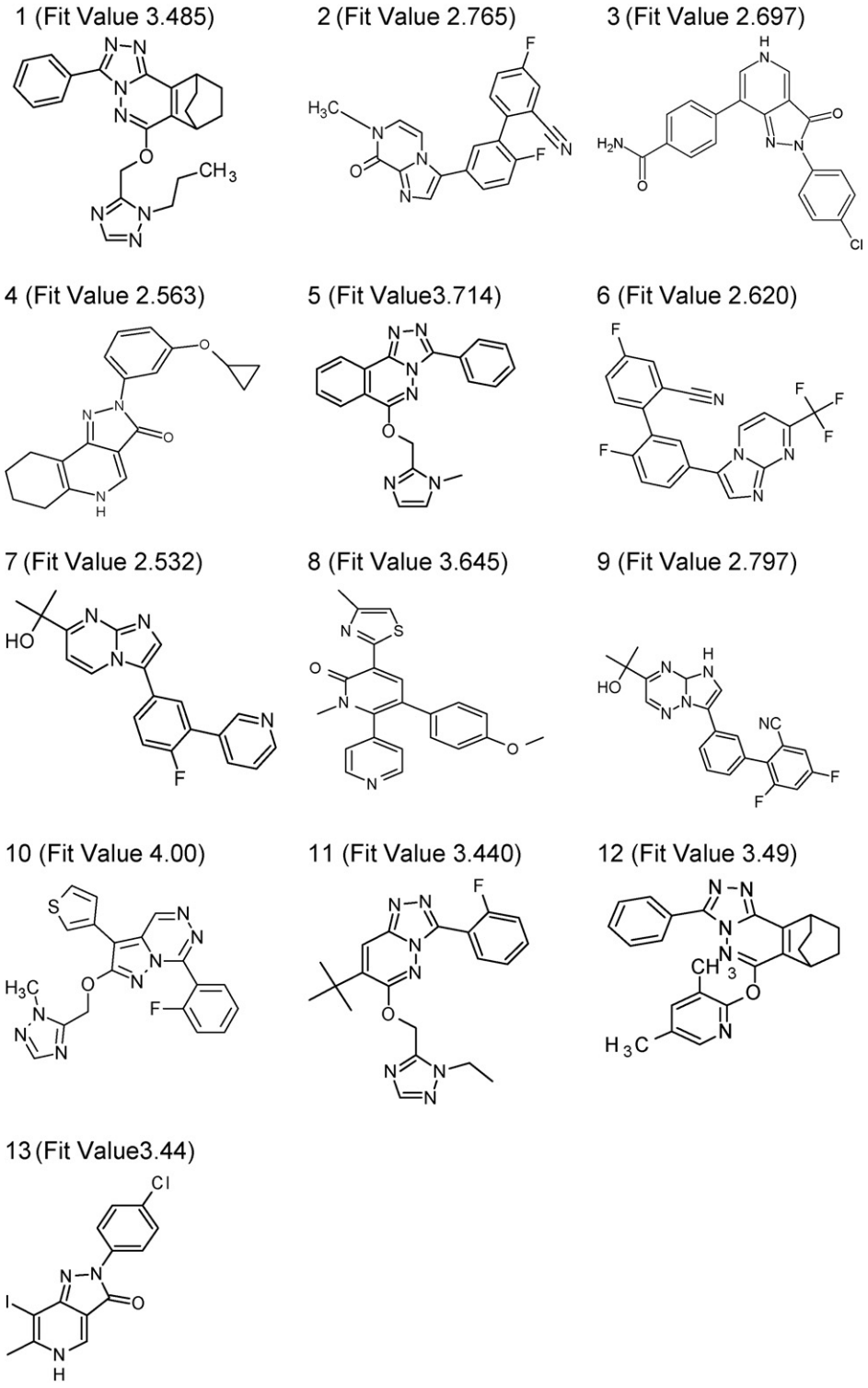

Fig. 3. Structures used for the generation of common feature hypothesis.

where "H^+/716", "HO^-/708", "CH_3/314..." and so on, are the probes and their numbering corresponding to their spatial positions, shown in Fig. 4.

The MFA model obtained had an explained variance of 80.8% and a predicted variance of 83.3%. Presence of probes OH^-/708 and H^+/716 with negative coefficients near position 4 of phenyl ring indicates that substitution by electronegative groups around position 4 of the 3-phenyl ring is not favorable as evidenced by decreased affinity in compound **6**. It is corroborated by the fact that fluorine substitution at two positions in compound **5** increases the affinity as compared to a non-substituted phenyl ring, evidenced in compound **64**. This is accounted to the fact that fluorine being electron withdrawing increases the positive nature of the phenyl ring. Hence structural modification around the phenyl ring system should be based on electronic parameters, representing electron withdrawing groups. The presence of a steric descriptor CH_3/484

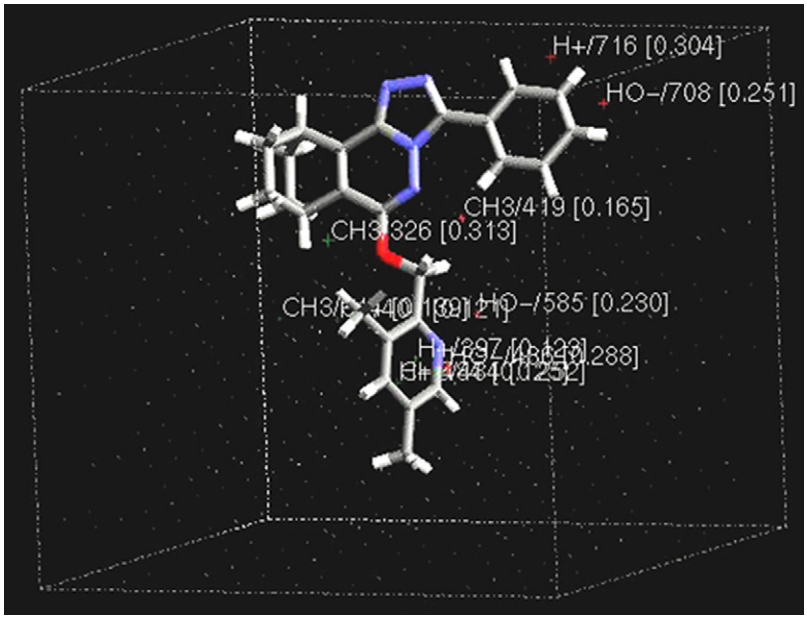

Fig. 4. Compound 14 enclosed inside a rectangular grid showing the 3D points of MFA, generated using Eq. (3).

with a positive coefficient at position 3 of the pyridyl moiety indicates that bulkier groups are favored at this position. Compounds **8**, **12**, **15**, **18**, **19**, **67** with bulky substitutions at position 3 show better affinity when compared to compounds **7**, **9**, **10**, and **11**, lacking bulky substitution at position 3. The presence of probe CH_3/314 with a positive coefficient near position 5 of the pyridyl group explains the basis for the high affinity compound **14** having methyl di-substitution at positions 3 and 5 of the pyridyl ring. Hence steric substituents are well tolerated around the aromatic heterocyclic (pyridyl) system. A CH_3/326 probe with a positive coefficient around the linker region connecting the pyridine moiety with triazole pthalazine core indicates the importance of a methyl spacer. Increase of the spacer carbon atom by one or two had a negative effect on affinity as shown in compounds **29** and **71**, respectively. These findings suggest that the MFA derived probe points are in good agreement with experimental structure–activity relationship (SAR) reported previously [15].

A receptor surface analysis (RSA) carried out on the generated psuedo receptor model showed that best rated QSAR model (shown in Eq. (2)) had an explained variance of 68.6% and a predicted variance of 69.2%.

The position of these descriptors, indicated by a number along with the descriptors, explains the nature of the required substituents. The descriptors VDW/3301 and VDW/3851 etc signify the van der Waals interaction energy of the molecule with the receptor at points 3301 and 3851, respectively. The descriptor TOT/3951 represents the added energy of electrostatic interaction and van der Waals interaction at point 3951. The view of the receptor surface model (RSM) embedded with the highest affinity compound **14** and the interactions are shown in Fig. 5(A)–(D). RSA reveals some important features that were not revealed by MFA. When the charge property was mapped on the receptor surface model, it shows a positive contour near the linker region and near the pthalzine core (Fig. 5(C)). This indicates that electronegative groups are essential at these positions. Hydrogen bonding propensity mapped on the receptor surface reveals the linker area to be involved in Hydrogen bonding interaction as a donor (Fig. 5(B)). Oxygen as a linker fulfills both the criteria above. Hydrophobicity mapped on the generated receptor reveals that pthalazine core to be involved in hydrophobic interaction except near the triazole nitrogen atoms and the linker oxygen atom, which are shown to be involved in polar interactions (Fig. 5(A)). The core region was shown to have the maximum favorable

$$\begin{aligned} pK_i = {} & 8.24896 + 7.562 \times \text{“VDW/1226”} - 5.65762 \times \langle -0.063257 - \text{“VDW/3301”} \rangle \\ & -18.6726 \times \langle \text{“VDW/3851”} + 0.256988 \rangle - 18.1343 \times \langle \text{“VDW/2751”} + 0.044931 \rangle \\ & +4.49784 \times \langle -0.25717 - \text{“VDW/4776”} \rangle + 21.5161 \times \langle \text{“TOT/3951”} + 0.017656 \rangle \\ & +10.2152 \times \langle -0.007871 - \text{“VDW/1426”} \rangle - 19.1306 \times \langle \text{“VDW/2176”} + 0.549454 \rangle \\ & -18.3264 \times \langle \text{“VDW/3851”} + 0.256355 \rangle \end{aligned} \quad (2)$$

$N_{\text{Training}} = 63$, $N_{\text{Test}} = 13$, optimal number of components (ONC) = 5,
$R^2 = 0.712$, adjusted R^2 (R^2_{adj}) = 0.686, Bs $R^2 = 0.660$, R^2_{cv} (q^2) = 0.739,
randomized $R^2 = 0.383$, SDEP = 0.358, LSE = 0.140, PRESS = 8.106,
$R^2_{\text{Pred}} = 0.692$, standard error of estimate (S) = 0.390, $\text{AVRES}_{\text{Test}} = 0.345$,
$\text{RMSE}_{\text{Test}} = 0.065$, $S_{\text{PRESS}} = 0.377$, $(R^2 - R^2_0)/R^2 = 0.02$, $k = 1$

The equation consists of nine descriptors. The terms in angle brackets such as ⟨“TOT/3951” + 0.017656⟩ are spline terms which are considered in the equation only when their value is greater than zero (with the cutoff level defined by the value of a).

interaction energy (Fig. 5(D)). Taken together these color renderings offer a qualitative way of examining the supra molecular interactions that occur at the ligand–receptor contact level.

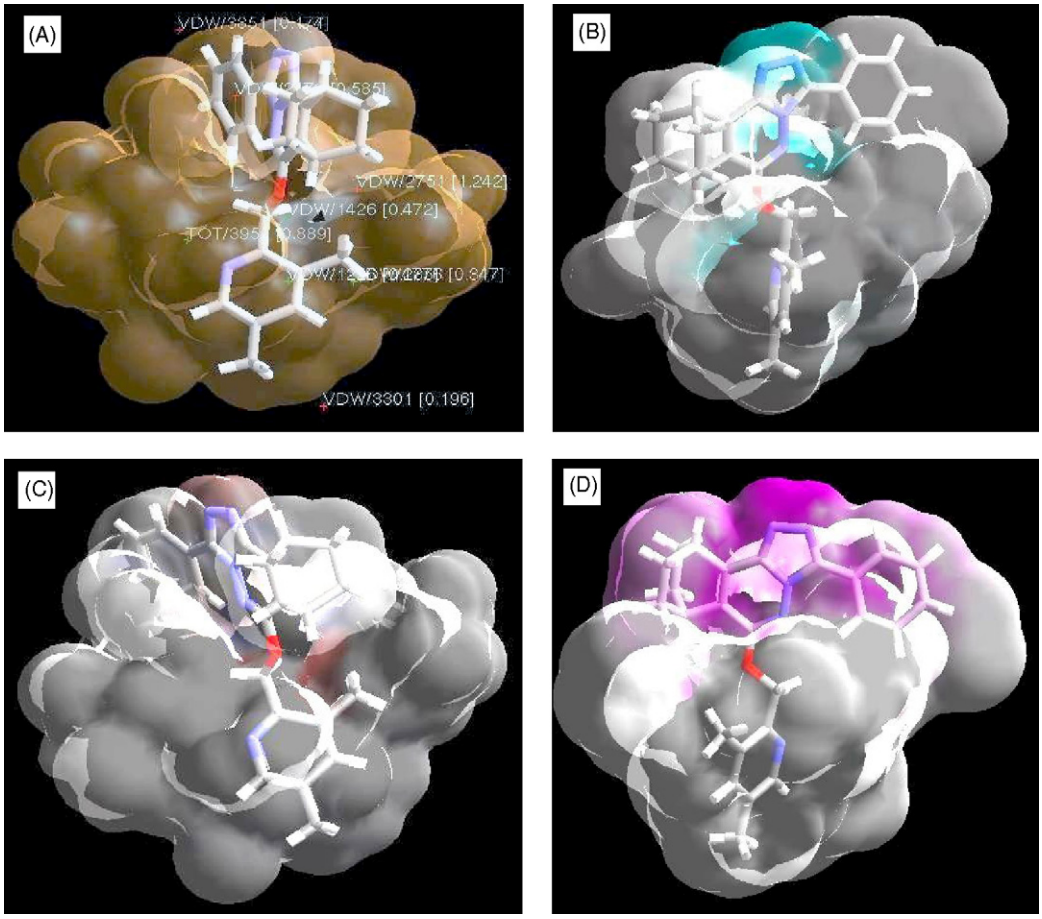

Fig. 5. A view of the pseudo receptor surface with high affinity compound **14** embedded inside. (A) Color rendering by hydrophobicity: brown (hydrophobic); gray (hydrophilic). (B) Color rendering by hydrogen bonding property; purple (hydrogen bond donor); light blue (hydrogen bond acceptors); white areas (no hydrogen bonding). (C) Color rendering by charge property: red areas (positively charged); blue areas (negatively charged), and white areas (neutral). (D) Color rendering showing favorable interactions (magenta) and unfavorable interaction (green).

The generated QSAR models were assessed for three important qualities namely goodness of fit, Model stability and Predictive ability. The reported parameters (given as foot note with Eqs. (1) and (2)) are explained variance (R^2_{adj}), square correlation coefficient (R^2), cross-validation R^2 (R^2_{cv} or q^2), predicted residual sum of squares (PRESS), standard error of prediction (S), standard deviation of error of prediction (SDEP), Bootstrap R^2 (Bs R^2), average of absolute values of residuals ($AVRES_{Test}$) and root mean square error ($RMSE_{Test}$). A regression diagnostic R^2 carried out to measure the goodness of fit of MFA and RSA models were statically high (0.821 and 0.712, respectively), shown in Fig. 6(A) and (B). Since R^2 tends to be inflated as the number of the descriptors increases (over fitting), R^2_{adj} was also evaluated for expository reasons. The value of R^2 and R^2_{adj} were close to each other in both the models.

Internal predictivity of the models was validated using a fully cross-validated leave-one-out (LOO) which performs superior

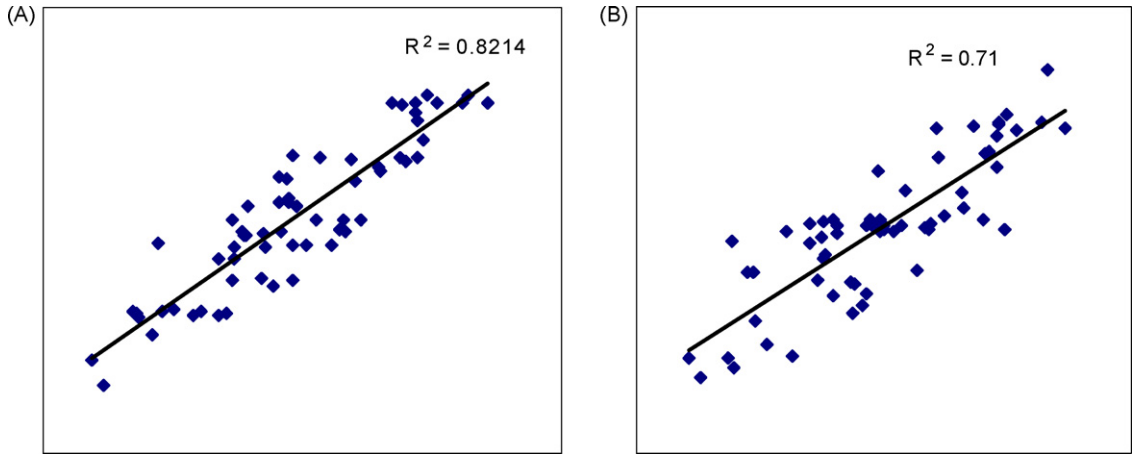

Fig. 6. (A) Plot of actual vs. calculated pK_i by MFA. (B) Plot of actual vs. calculated pK_i by RSA.

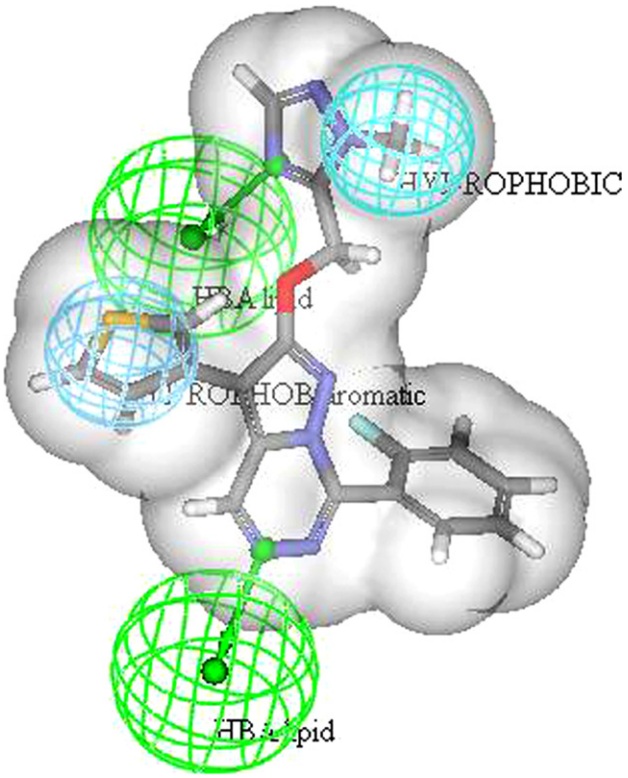

Fig. 7. "Target-specific pharamacophore" mapped on the high affinity ligand 11 together with shape feature, "inclusion volume", depicted in gray (image rendered using Ds Visualizer, Accelrys Inc.).

when compared to the standard regression only cross validation [20]. Obtained $R^2_{cv}(q^2)$ values of 0.814 (MFA) and 0.739 (RSA) assure the predictive ability of the models. To ensure the absence of chance correlation, the developed models were also subjected to *Y*-randomization test by scrambling the dependent variable set, which were in turn used to generate QSAR models corresponding to a 90% confidence level. Randomized R^2 values of 0.462 (MFA) and 0.383 (RSA) apparently signify the stability of the models. Randomization and LOO cross validation do not guarantee a predictive model, hence the predictive ability and extensibility of the models were established using an external test set consisting of 13 compounds, not considered during the model generation process [34].

The predictive power of the models were calculated using the formula:

$$R^2_{\text{Pred}} = \frac{\text{SD} - \text{PRESS}}{\text{SD}} \tag{3}$$

where SD is the sum of square deviations between the biological activities of each molecule in the test and the mean activity of the training set molecules and PRESS is the sum of square deviations between the predicted and the actual activities of molecules in the test set. Tropsha et al. [34] have proposed certain guidelines apart from R^2_{Pred} that should be considered to estimate the predictive power of a QSAR model. They recommended the use of the following formula for illustrating the predictive ability:

$$\frac{R^2 - R_0^2}{R^2} < 0.1 \quad \text{or} \quad \frac{R^2 - R_0^{2'}}{R^2} < 0.1 \tag{4}$$

and

$$k \text{ or } k' \text{ close to } 1 \tag{5}$$

where R^2 represents the square correlation coefficient between the predicted and observed activities. R_0^2 and $R_0^{2'}$ are quantities characterizing the correlation between predicted vs. observed and observed vs. predicted activity, respectively, with *Y*-intercept set to zero and k, k' their corresponding slopes. More details of the formula are covered elsewhere [19] and are not elaborated for reasons of brevity. The overall statistical quality index as evident from the footnotes stated with Eqs. (1) and (2) reveal that both MFA and RSA models satisfy the acceptability criteria for a valid QSAR model ($R^2 > 0.6$, $q^2 > 0.5$, and $R^2_{\text{Pred}} > 0.5$).

It was found that two independent models RSA and MFA identified the same outliers (details provided in supplementary information). These two compounds appeared as outliers in both training and test sets, hence omission of these compounds from the dataset was considered. Particular attention was paid to reason out this inhomogeneity, as omission of outliers from dataset can create a statistical artifact. Descriptor-based *K*-means clustering performed earlier for the division of training set and test set reveals that outlier compounds share the same descriptor domain space as the rest in the training set, hence the possibility of being an *X* dependent outlier was ruled out. In light of this observation, we are convinced that these compounds should be *X*/*Y* relation outliers having a relationship that is unable to fit with the current equation and hence the removal of these outliers from the model building process was considered [35,36].

3.2. A subtype selective pharmacophore model

The pharmacophore model investigated in this study is the first report of a systematically studied α_3 subtype selective model. The results of the top 10 hypotheses are given in Table 2 with scores ranging from 125.796 to 119.259. The highest ranking hypothesis, as deduced by the Catalyst program, reveals that the minimal pharmacophoric features required for α_3 subtype selectivity are one HYDROPHOBIC aromatic (X), one HYDROPHOBIC aliphatic (Z) and two HBA lipids (H). The ranking of hypotheses is based on how well the reference compounds fit the proposed pharmacophore and the rarity of the pharmacophore [30]. The higher the ranking, it

Table 2
Results of the common feature hypothesis run

1	XZHH rank: 125.796	DH: 1111111111111	PH: 0000000000000	Max Fit: 4
2	XZHA rank: 123.47	DH: 1111111111111	PH: 0000000000000	Max Fit: 4
3	XZHA rank: 123.196	DH: 1111111111111	PH: 0000000000000	Max Fit: 4
4	XZHH rank: 122.971	DH: 1111111111111	PH: 0000000000000	Max Fit: 4
5	XZHH rank: 121.859	DH: 1111111111111	PH: 0000000000000	Max Fit: 4
6	XZHA rank: 120.371	DH: 1111111111111	PH: 0000000000000	Max Fit: 4
7	XZHA rank: 120.371	DH: 1111111111111	PH: 0000000000000	Max Fit: 4
8	XZHH rank: 119.826	DH: 1111111111111	PH: 0000000000000	Max Fit: 4
9	XZHA rank: 119.332	DH: 1111111111111	PH: 0000000000000	Max Fit: 4
10	XZHA rank: 119.259	DH: 1111111111111	PH: 0000000000000	Max Fit: 4

Note: Hydrophobic aromatic (X); hydrophobic aliphatic (Z); HBA lipid (H); hydrogen bond acceptor (A); DH: direct hit; PH: partial hit.

```
P14867|GBRA1_HUMAN   MDAHACPLKFGSYAYTRAEVVYEWTREPARSVVVAEDGSRLNQYDLLGQTVDSGIVQSST 207
P47869|GBRA2_HUMAN   MDAHSCPLKFGSYAYTTSEVTYIWTYNASDSVQVAPDGSRLNQYDLLGQSIGKETIKSST 234
P31644|GBRA5_HUMAN   MDAHACPLKFGSYAYPNSEVVYVWTNGSTKSVVVAEDGSRLNQYHLMGQTVGTENISTST 210
P34903|GBRA3_HUMAN   MDVHACPLKFGSYAYTTAEVVYSWTLGKNKSVEVAQDGSRLNQYDLLGHVVGTEIIRSST 231
P48169|GBRA4_HUMAN   MDGHACPLKFGSYAYPKSEMIYTWTKGPEKSVEVPKESSSLVQYDLIGQTVSSETIKSIT 240
Q16445|GBRA6_HUMAN   MDGHACPLKFGSYAYPKSEIIYTWKKGPLYSVEVPEESSSLLQYDLIGQTVSSETIKSNT 205
                     ** *:**********. :*: * *.     ** *. :.* * **.*:*: :..  : : *

P14867|GBRA1_HUMAN   GEYVVMTTHFHLKRKIGYFVIQTYLPCIMTVILSQVSFWLNRESVPARTVFGVTTVLTMT 267
P47869|GBRA2_HUMAN   GEYTVMTAHFHLKRKIGYFVIQTYLPCIMTVILSQVSFWLNRESVPARTVFGVTTVLTMT 294
P31644|GBRA5_HUMAN   GEYTIMTAHFHLKRKIGYFVIQTYLPCIMTVILSQVSFWLNRESVPARTVFGVTTVLTMT 270
P34903|GBRA3_HUMAN   GEYVVMTTHFHLKRKIGYFVIQTYLPCIMTVILSQVSFWLNRESVPARTVFGVTTVLTMT 291
P48169|GBRA4_HUMAN   GEYIVMTVYFHLRRKMGYFMIQTYIPCIMTVILSQVSFWINKESVPARTVFGITTVLTMT 300
Q16445|GBRA6_HUMAN   GEYVIMTVYFHLQRKMGYFMIQIYTPCIMTVILSQVSFWINKESVPARTVFGITTVLTMT 265
                     *** :**.:***:**:***:** * ***************:*:**********:******* 
```

Fig. 8. A representative subset illustrating the degree of conservation of the putative BDZ pocket. All the human $GABA_A$ α subunits were retrieved from Swiss-Prot data bank and was numbered after editing the signaling part. Conserved residues corresponding to the "message" part are labeled in blue, and residues corresponding to the "address" part are shown in red. Consensus key: fully conserved residue (*); strong conservation (:), weak conservation (.).

is less likely that the molecules fit the hypothesis by chance correlation [37].

A careful examination of the fit values (Fig. 3) reveals that, compound 10 reported with Best "Fit Value", also happens to be the molecule with the best K_i value [28]. Hence the spatial information of this compound was reformulated into a shape query using Catalyst functionality, Cat Shape. This shape feature approximately characterizes the size of the putative ligand-binding volume, which we term as "Inclusion volume". This represents the volume that has to be occupied by the ligand, in contrast to "Excluded Volume" which defines a region that is occupied by the receptor. Hence, the obtained pharmacophore was spatially constrained in order to yield a "Target specific pharamacophore", shown in Fig. 7.

3.3. A binding mode consistent with "Message – Address" concept

A composite hypothetical-binding pocket defining the sub-sites can be proposed in terms of 3D QSAR and pharmacophore models discussed above. MFA, RSA and pharmacophore studies reveal that the phenyl ring attached to the pthalazine core is characterized by a hydrophobic feature. MFA studies also reveal that substitutions around the phenyl ring are not favorable and this has been reflected in our pharmacophoric model as a shape constraint. Hydrogen bonding propensity revealed by RSA shows the triazole nitrogen to be involved in hydrogen bonding interactions; this particular feature was also mapped by Catalyst as an HBA lipid feature. RSA studies reveal the bicyclic ring system fused to the pthalazine moiety to be involved in lipophilic interaction. It was evident from MFA studies that a methyl spacer connecting the pyridine moiety with triazole pthalazine core plays an important role. This linker should interact with the lipophilic channel like region known to exist at the interface between α and γ subunits in the $GABA_A$ receptor where the benzodiazepine binding site is most likely to be located [38]. Quite unexpectedly, RSA generated psuedo receptor reveals only a small portion of favorable interactions in the vicinity of the substituted areas. These observations essentially reiterate a key tenet of the "Message–Address" concept, originally proposed by Schwyzer [39] and implemented in various studies [40–43]. We presume that the conformationally constrained pthalazine core mimics the "Message" part that is crucial for initial binding, brings about a conformational change in the pre M1 region [44]. (transduction or coupling) and place the key "Address" region in close proximity to amino acid residues, critical for the enhancement of channel opening and ion flux (gating). This "Address" component confers selectivity and additional binding.

It is apparent that the difference in the binding affinity of a ligand with respect to different paralogous $GABA_A$ α subunits is eventually due to the difference in their amino acid sequences. Thus, elucidating the differentiating patterns of residue conservation among the different functional subtypes can be employed to identify residues expected to be involved in functional specificity. Hence, we carried out a multiple sequence alignment using CLUSTAL-W [45] on the mature sequences of the Human alpha subunits retrieved from Swiss Prot [46] to identify the conservation patterns. The results show that the signature residues (Y160, Y210, S186 and R187 on the α1 subunit) involved in BDZ binding as proposed by Hong Xue et al. [47] are highly conserved among all paralogous alpha subtypes. Residues Y160, Y210, S186 are highly conserved and R187 is semi conserved (shown in Fig. 8). This reiterates the fact that a highly conserved binding pocket, exists in common for all paralogous subtypes which recognizes the "Message" component.

Though it seems too early to speculate which amino acids correspond to the "address" component, we presume that the few non conserved residues Thr202 in α_2, Arg204 in α_3 and Thr205 in α_5, known to exist close to the BDZ pocket with varying degrees of polarity, contribute for the selectivity of the "Address" component. Further, Russel et al. [15] have also shown that PSA and pK_a are distinguishing physicochemical properties conferring selectivity. On the basis of these findings we hypothesize that these non-conserved polar residues account for selectivity.

Analyzing the spatial disposition of the residues based on sequence conservation together with the associated physicochemical properties derived using 3D QSAR and pharmacophore techniques lend credence to this hypothesis. Though the model is valid in a qualitative context and proves a step closer towards the construction of a detailed molecular model of the BDZ-binding site, we emphasize the need to test this hypothesis on recombinant receptors combined with the analysis of point mutations and amino acid scanning techniques. It is hoped that such a combination could provide an ultimate insight in distinguishing the respective roles of amino acids contributing for binding and selectivity. Based on these observations, a hypothetical-binding pocket along with sub-sites has been derived as shown in Fig. 9.

The sub-sites are labeled as L1, H1, A1 and H2, where L1 represents a lipophilic site that involves in a hydrophobic interaction, H1 as hydrogen bond donor, A1 represents a sterically restricted region as revealed by SAR [15], and a hydrogen bond donor site H2, interacting with the linker oxygen. It is worth noting that the binding pocket described here complements and extends the previous pharmacophoric model developed by Cook

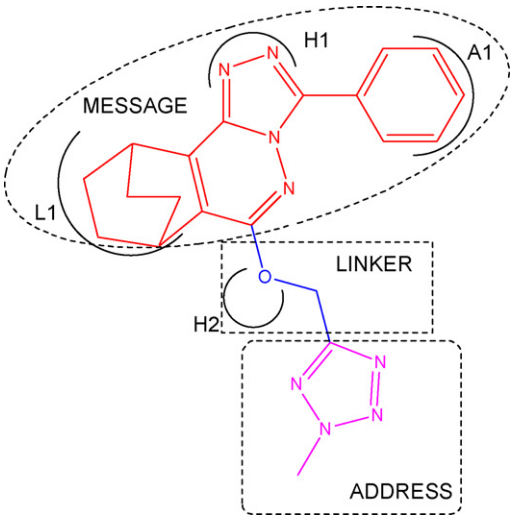

Fig. 9. A hypothetical-binding pocket along with sub-sites.

et al. [48]. This implicates a common mechanism for channel modulation, at the BDZ-binding site, even by distinct class of compounds.

3.4. Pharmacophore validation and scaffold hopping

The success of pharmacophore-based virtual screening (PBVS) relies largely on the accuracy and specificity of the pharmacophore query employed. Keeping in mind the caveats regarding false positives during virtual screening, a statistical approach was used to gauge the enrichment ability of the "target-specific pharmacophore". A "Decoy database" seeded with both selective and non-selective compounds were created using the CAT Info module of Catalyst. Diazepam, Zolidipem, Cl-218, 872, ROD185 and Abecarnil, known to be non selective against $\alpha 3$, were included as negative controls. Inclusion of such negative controls helps in validating the quality of the generated pharmacophore and the virtual screening process. The "target-specific pharmacophore" model was used to query the "Decoy database" using the fast flexible search option. The quality of the pharmacophore was calculated using different statistical metrics namely selectivity, sensitivity and enrichment [49]:

$$\text{Selectivity} = \frac{\text{TP}}{\text{TP} + \text{FN}}$$

$$\text{Sensitivity (recall)} = \frac{\text{TP}}{\text{TP} + \text{FP}}$$

$$\text{Enrichment} = \frac{\text{TP}/\text{TP} + \text{FP}}{\text{TP} + \text{FN}/N}$$

TP, FN, and FP stand for true positive, false negative and false positive, respectively. N represents the total number of compound in the Decoy database.

The "Target-specific pharmacophore" had 65% sensitivity in recalling true positives, 100% selectivity in avoiding false positives and an enrichment value of 65%. These values suggest a highly reliable "Target-specific pharmacophore" that could be used for screening databases.

Scaffold hopping for the identification of newer chemotypes was done using the "Target-specific pharmacophore" framework together with distance constraints as a query.

May bridge 2004 database (59,652 compounds) was searched using the Fast Flexible search option. The main challenge during virtual screening is to choose a subset of focused compounds. A two stage filtering process based on "Drug likeness" and "Similarity principle" criteria was used to create a focused subset. Lipinski's "Rule of 5", a well known rule-of-thumb was used for initial filtering [32] (Filter 1). Further, a similarity-based PCA clustering using multiple reference structures was used to cluster the candidate hits (Filter 2) [33].

To evaluate the structural similarity of the hits with reference compounds, the high dimensional descriptor space was calculated and was scaled to a low dimensional space, using Cerius^2 PCA. The loading plot obtained (Fig. 11) was used to evaluate the structural similarity of the hits with known reference compounds. Those hits, not distributed among the known selective compounds, possess lower molecular similarity and were discarded, as they are less favorable lead candidates (shown in Fig. 10).

This protocol could be regarded as the most comprehensive and accurate approach to validate and prioritize hits in a ligand-based virtual screening process, since a ligand-based design capitalize on the fact that ligands similar to an active ligand are more likely to be active than random ligands, referred to as "Neighborhood

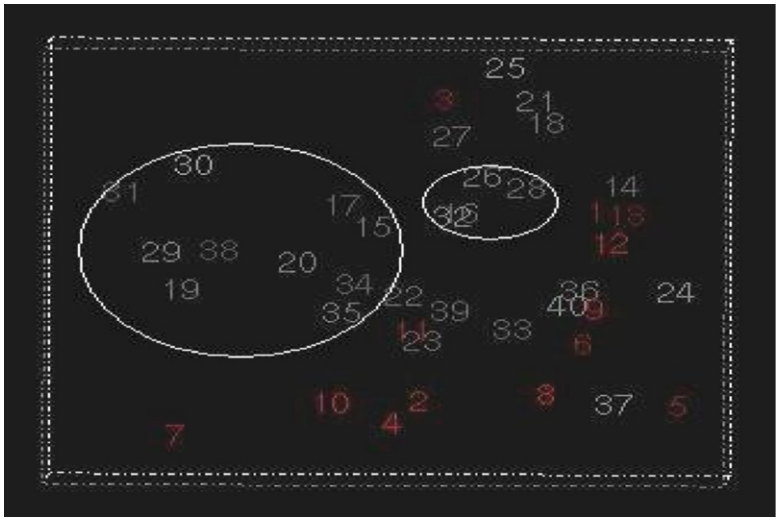

Fig. 10. PCA plot showing the degree of similarity of the hits (white) obtained after virtual screening with those of the reference compounds (red). The compounds inside the circled regions represent outliers.

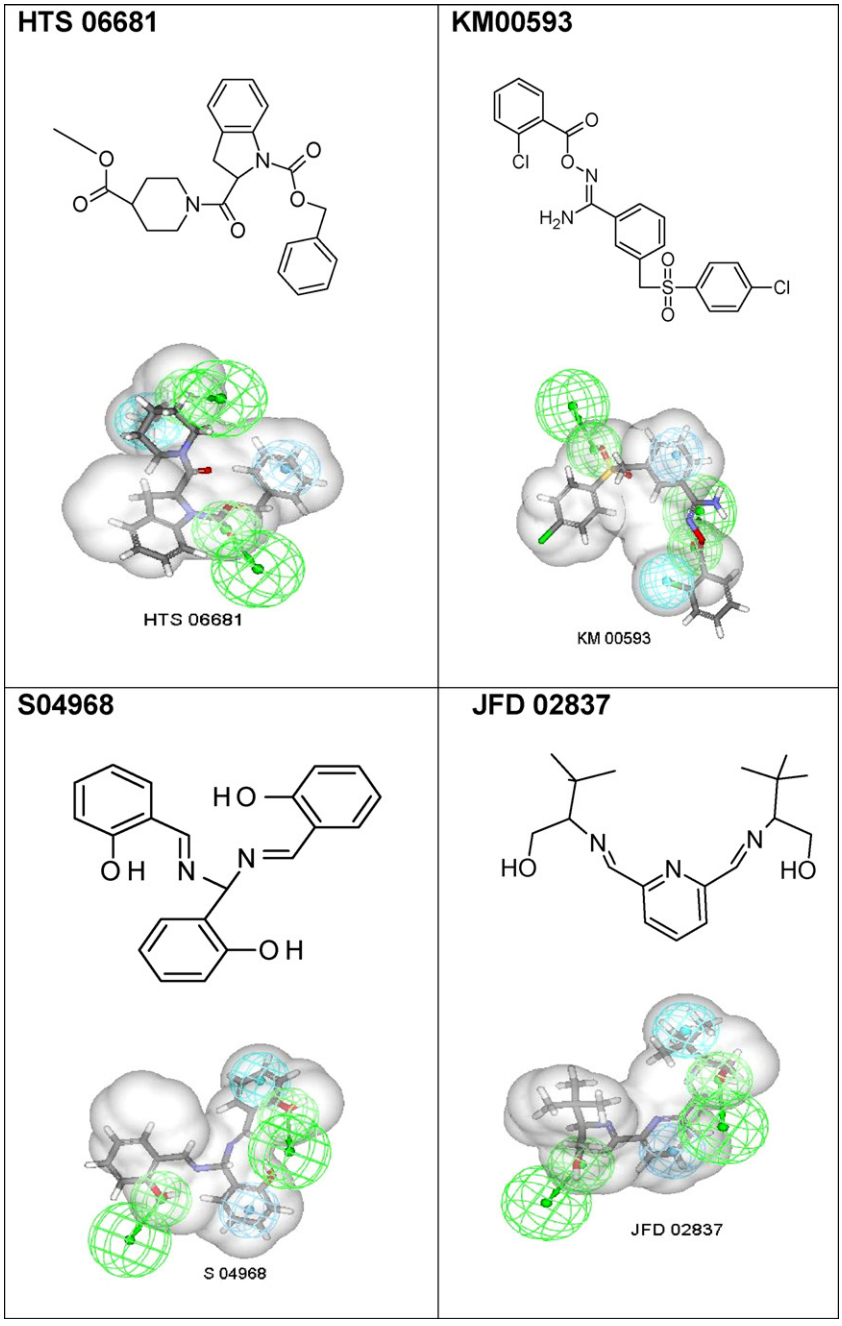

Fig. 11. Examples of hits with new scaffolds obtained after post-filtering.

behavior" [50]. Some examples of hits obtained after filtering are shown in Fig. 11.

4. Conclusion

The development of subtype selective agonists for the treatment of epilepsy is an active area of drug discovery research. In this work, two different molecular modeling techniques were employed to address affinity and selectivity. The strength of the present study is the interpretability of the 3D QSAR results in structural terms in exploring the requirements for affinity. Properties that account for the biological response as inferred from our 3D QSAR results are consistent with the previously reported SAR data.

The obtained "Target-specific pharmacophore" highlights the chemical functionalities required for $GABA_A$ α_3 receptor subtype selectivity. An attempt to rationalize the binding mode in concert with "Message–Address" concept could facilitate in delineating the basis of ligand selectivity and could bring about important pharmacophoric considerations that could aid in the design of highly selective novel leads with reduced side effect profile. Scaffold hopping done for the identification of newer chemotypes was enriched using a robust filtering process for the creation of a focused subset of potential leads.

Acknowledgements

The authors thank Council for Scientific and Industrial Research (CSIR), New Delhi, for providing financial grant under Mission

Mode Program CMM0017 and Accelrys support group for their valuable suggestions. R.S.K. Vijayan thanks CSIR, New Delhi for awarding Senior Research Fellowship.

Appendix A. Supplementary data

Supplementary data associated with this article can be found, in the online version, at doi:10.1016/j.jmgm.2008.05.003.

References

[1] P. Kahnberg, M.H. Howard, T. Liljefors, M. Nielsen, E.O. Nielsen, O. Sterner, I.J. Pettersson, The use of a pharmacophore model for identification of novel ligands for the benzodiazepine binding site of the $GABA_A$ receptor, J. Mol. Graphics Model. 23 (3) (2004) 253–261.

[2] J.R. Trudell, E. Bertaccini, Comparative modeling of a $GABA_A$ alpha1 receptor using three crystal structures as templates, J. Mol. Graphics Model. 23 (1) (2004) 39–49.

[3] E.R. Korpi, G. Gründer, H. Lüddens, Drug interactions at $GABA_A$ receptors, Prog. Neurobiol. (67) (2002) 113–159.

[4] S.C. Goodacre, L.J. Street, D.J. Hallett, J.M. Crawforth, S. Kelly, A.P. Owens, W.P. Blackaby, R.T. Lewis, J. Stanley, A.J. Smith, P. Ferris, B. Sohal, S.M. Cook, A. Pike, N. Brown, K.A. Wafford, G. Marshall, J.L. Castro, J.R. Atack, Imidazo[1,2-*a*] pyrimidines as functionally selective and orally bioavailable GABA(A)alpha2/alpha3 binding site agonists for the treatment of anxiety disorders, J. Med. Chem. 49 (2006) 35–38.

[5] D. Berezhnoy, Y. Nyfeler, A. Gonthier, H. Schwob, M. Goeldner, E. Sigel, On the benzodiazepine binding pocket in $GABA_A$ receptors, J. Biol. Chem. 279 (5) (2004) 3160–3168.

[6] C. Grunwald, C. Rundfeldt, H.J. Lankau, T. Arnold, N. Hofgen, R. Dost, U. Egerland, H.J. Hofmann, K. Unverferth, Synthesis, pharmacology, and structure–activity relationships of novel imidazolones and pyrrolones as modulators of $GABA_A$ receptors, J. Med. Chem. 49 (2006) 1855–1866.

[7] U. Rudolph, F. Crestani, D. Benke, I. Brunig, J.A. Benson, J.M. Fritschy, J.R. Martin, H. Bluethmann, H. Mohler, Benzodiazepine actions mediated by specific gamma-aminobutyric acid(A) receptor subtypes, Nature (London) 401 (6755) (1999) 796–800.

[8] R.M. McKernan, T.W. Rosahl, D.S. Reynolds, C. Sur, K.A. Wafford, J.R. Atack, S. Farrar, J. Myers, G. Cook, P. Ferris, L. Garrett, L. Bristow, G. Marshall, A. Macaulay, N. Brown, O. Howell, K.W. Moore, R.W. Carling, L.J. Street, J.L. Castro, C.I. Ragan, G.R. Dawson, P.J. Whiting, Sedative but not anxiolytic properties of benzodiazepines are mediated by the GABA (A) receptor alpha1 subtype, Nat. Neurosci. 3 (6) (2000) 587–592.

[9] K. Low, F. Crestani, R. Keist, D. Benke, I. Brunig, J.A. Benson, J.M. Fritschy, T. Rulicke, H. Bluethmann, H. Mohler, U. Rudolph, Molecular and neuronal substrate for the selective attenuation of anxiety, Science 290 (5489) (2000) 131–134.

[10] Accelrys, Ceruis^2 Version 4.10, Accelrys Inc., CA, USA. http://www.accelrys.com (Online).

[11] Accelrys, Catalyst Version 11, Accelrys Inc., CA, USA. http://www.accelrys.com (Online).

[12] Chem Draw Ultra Version 5.0, is a Program of Cambridge Soft Corporation, USA, Cambridge, MA, USA. http://www.cambridgesoft.com (Online).

[13] SPSS, Statistical Software of SPSS Inc., Chicago, IL, USA. http://www.spss.com (Online).

[14] N. Ghoshal, P.K. Mukherjee, 3-D-QSAR of *N*-substituted 4-amino-3,3-dialkyl-2(3*H*)-furanone GABA receptor modulators using molecular field analysis and receptor surface modelling study, Bioorg. Med. Chem. Lett. 14 (1) (2004) 103–109.

[15] M.G. Russell, R.W. Carling, J.R. Atack, F.A. Bromidge, S.M. Cook, P. Hunt, C. Isted, M. Lucas, R.M. McKernan, A. Mitchinson, K.W. Moore, R. Narquizian, A.J. Macaulay, D. Thomas, S.A. Thompson, K.A. Wafford, J.L. Castro, Discovery of functionally selective 7,8,9,10-tetrahydro-7,10-ethano-1,2,4-triazolo[3,4-*a*]phthalazines as $GABA_A$ receptor agonists at the alpha 3 subunit, J. Med. Chem. 48 (2005) 1367–1383.

[16] J.T. Leonard, K. Roy, On selection of training and test sets for the development of predictive QSAR models, QSAR Combust. Sci. 25 (3) (2006) 235–251.

[17] P.M. Dean, Comparative molecular field analysis, in: P.M. Dean (Ed.), Molecular Similarity in Drug Design, Blackie Academic & Professional, Glasgow, 1995 , p. 295.

[18] H. Yuan, A. Parrill, Cluster analysis and three-dimensional QSAR studies of HIV-1 integrase inhibitors, J. Mol. Graphics Model. 23 (4) (2005) 317–328.

[19] A. Golbraikh, M. Shen, Z. Xiao, Y.D. Xiao, K.H. Lee, A. Tropsha, Rational selection of training and test sets for the development of validated QSAR models, J. Comput. Aided Mol. Design 17 (2–4) (2003) 241–253.

[20] D. Rogers, Some theory and examples of genetic function approximation with comparison to evolutionary techniques, in: J. Devillers (Ed.), Genetic Algorithm in Molecular Modelling, Academic Press, London, 1996, p. 92.

[21] R.W. Carling, K.W. Moore, L.J. Street, D. Wild, C. Isted, P.D. Leeson, S. Thomas, D. O'Connor, R.M. McKernan, K. Quirk, S.M. Cook, J.R. Atack, K.A. Wafford, S.A. Thompson, G.R. Dawson, P. Ferris, J.L. Castro, 3-Phenyl-6-(2-pyridyl)methyloxy-1,2,4-triazolo[3,4-*a*]phthalazines and analogues: high-affinity gamma-aminobutyric acid-A benzodiazepine receptor ligands with alpha 2, alpha 3, and alpha 5-subtype binding selectivity over alpha 1, J. Med. Chem. 47 (7) (2004) 1807–1822.

[22] R.W. Carling, A. Madin, A. Guiblin, M.G. Russell, K.W. Moore, A. Mitchinson, B. Sohal, A. Pike, S.M. Cook, I.C. Ragan, R.M. McKernan, K. Quirk, P. Ferris, G. Marshall, S.A. Thompson, K.A. Wafford, G.R. Dawson, J.R. Atack, T. Harrison, J.L. Castro, L.J. Street, 7-(1,1-Dimethylethyl)-6-(2-ethyl-2*H*-1,2,4-triazol-3-ylmethoxy)-3-(2-fluorophenyl)-1,2,4-triazolo[4,3-*b*] pyridazine: a functionally selective gamma-aminobutyric acid(A) (GABA(A)) alpha2/alpha3-subtype selective agonist that exhibits potent anxiolytic activity but is not sedating in animal models, J. Med. Chem. 48 (23) (2005) 7089–7092.

[23] M.G. Russell, R.W. Carling, L.J. Street, D.J. Hallett, S. Goodacre, E. Mezzogori, M. Reader, S.M. Cook, F.A. Bromidge, R. Newman, A.J. Smith, K.A. Wafford, G.R. Marshall, D.S. Reynolds, R. Dias, P. Ferris, J. Stanley, R. Lincoln, S.J. Tye, W.F. Sheppard, B. Sohal, A. Pike, M. Dominguez, J.R. Atack, J.L. Castro, Discovery of imidazo[1,2-*b*][1,2,4]triazines as GABA(A) alpha2/3 subtype selective agonists for the treatment of anxiety, J. Med. Chem. 49 (4) (2006) 1235–1238.

[24] S.C. Goodacre, D.J. Hallett, R.W. Carling, J.L. Castro, D.S. Reynolds, A. Pike, K.A. Wafford, R. Newman, J.R. Atack, L.J. Street, Imidazo[1,2-*a*]pyrazin-8-ones, imidazo[1,2-*d*][1,2,4]triazin-8-ones and imidazo[2,1-*f*][1,2,4]triazin-8-ones as $\alpha 2/\alpha 3$ subtype selective GABAA agonists for the treatment of anxiety, Bioorg. Med. Chem. Lett. 16 (6) (2006) 1582–1585.

[25] S.C. Goodacre, L.J. Street, D.J. Hallett, J.M. Crawforth, S. Kelly, A.P. Owens, W.P. Blackaby, R.T. Lewis, J. Stanley, A.J. Smith, P. Ferris, B. Sohal, S.M. Cook, A. Pike, N. Brown, K.A. Wafford, G. Marshall, J.L. Castro, J.R. Atack, Imidazo[1,2-*a*]pyrimidines as functionally selective and orally bioavailable GABA(A)alpha2/alpha3 binding site agonists for the treatment of anxiety disorders, J. Med. Chem. 49 (1) (2006) 35–38.

[26] A. Mitchinson, J.R. Atack, P. Blurton, R.W. Carling, J.L. Castro, K.S. Curley, M.G. Russell, G. Marshall, R.M. McKernan, K.W. Moore, R. Narquizian, A. Smith, L.J. Street, S.A. Thompson, K. Wafford, 2,5-Dihydropyrazolo [4,3-*c*] pyridin-3-ones: functionally selective benzodiazepine binding site ligands on the $GABA_A$ receptor, Bioorg. Med. Chem. Lett. 14 (13) (2004) 3441–3444.

[27] W.P. Blackaby, J.R. Atack, F. Bromidge, R. Lewis, M.G. Russell, A. Smith, K. Wafford, R.M. McKernan, L.J. Street, J.L. Castro, Pyrazolopyridinones as functionally selective GABAA ligands, Bioorg. Med. Chem. Lett. 15 (22) (2005) 4998–5002.

[28] R.W. Carling, M.G. Russell, K.W. Moore, A. Mitchinson, A. Guiblin, A. Smith, K.A. Wafford, G. Marshall, J.R. Atack, L.J. Street, 2,3,7-Trisubstituted pyrazolo[1,5-*d*][1,2,4]triazines: functionally selective $GABA_A$ alpha3-subtype agonists, Bioorg. Med. Chem. Lett. 16 (13) (2006) 3550–3554.

[29] I. Collins, C. Moyes, W.B. Davey, M. Rowley, F.A. Bromidge, K. Quirk, J.R. Atack, R.M. McKernan, S.A. Thompson, K. Wafford, G.R. Dawson, A. Pike, B. Sohal, N.N. Tsou, R.G. Ball, J.L. Castro, 3-Heteroaryl-2-pyridones: benzodiazepine site ligands with functional selectivity for alpha 2/alpha 3-subtypes of human GABA(A) receptor-ion channels, J. Med. Chem. 45 (9) (2002) 1887–1900.

[30] D. Barnum, J. Greene, A. Smellie, P. Sprague, Identification of common functional configurations among molecules, J. Chem. Inform. Comput. Sci. 36 (3) (1996) 563–571.

[31] A. Smellie, S.L. Teig, P. Towbin, Poling, Promoting conformational variation, J. Comput. Chem. 16 (1994) 171–187.

[32] C.A. Lipinski, F. Lombardo, B.W. Dominy, P.J. Feeney, Experimental and computational approaches to estimate solubility and permeability in drug discovery and development settings, Adv. Drug Del. Rev. 46 (2001) 3–26.

[33] T.M. Steindl, C.E. Crump, F.G. Hayden, T. Langer, Pharmacophore modeling, docking, and principal component analysis based clustering: combined computer-assisted approaches to identify new inhibitors of the human rhinovirus coat protein, J. Med. Chem. 48 (2005) 6250–6260.

[34] A. Golbraikh, A. Tropsha, Beware of q^2, J. Mol. Graphics Model. 20 (4) (2002) 269–276.

[35] E. Furusjo, A. Svenson, M. Rahmberg, M. Andersson, The importance of outlier detection and training set selection for reliable environmental QSAR predictions, Chemosphere 63 (1) (2006) 99–108.

[36] R.P. Verma, C. Hansch, An approach toward the problem of outliers in QSAR, Bioorg. Med. Chem. 13 (15) (2005) 4597–4621.

[37] A. Hirashima, M. Morimoto, H. Ohta, E. Kuwano, E. Taniguchi, M. Eto, Three-dimensional common-feature hypotheses for octopamine agonist. 1-Arylimidazolidine-2-thiones, Int. J. Mol. Sci. 3 (2002) 56–68.

[38] P. Kahnberg, E. Lager, C. Rosenberg, J. Schougaard, L. Camet, O. Sterner, E. Østergaard Nielsen, M. Nielsen, T. Liljefors, Refinement and evaluation of a pharmacophore model for flavone derivatives binding to the benzodiazepine site of the GABA(A) receptor, J. Med. Chem. 45 (2002) 4188–4201.

[39] R. Schwyzer, ACTH: a short introductory review, Ann. NY Acad. Sci. 297 (1977) 3–26.

[40] P.S. Portoghese, M. Sultana, A.E. Takemori, Design of peptidomimetic delta opioid receptor antagonists using the message–address concept, J. Med. Chem. 33 (6) (1990) 1714–1720.

[41] Y. Peng, S.M. Keenan, Q. Zhang, V. Kholodovych, W.J. Welsh, 3D-QSAR comparative molecular field analysis on opioid receptor antagonists: pooling data from different studies, J. Med. Chem. 48 (5) (2005) 1620–1629.

[42] I.J. McFadyen, T.G. Metzger, M.G. Paterlini, D.M. Ferguson, Exploring the unique pharmacology of a novel opioid receptor, ZFOR1, using molecular modeling and the 'message–address' concept, Protein Eng. 14 (12) (2001) 953–960.

[43] B.E. Kane, B. Svensson, D.M. Ferguson, Molecular recognition of opioid receptor ligands, AAPS J. 8 (1) (2006) E126–E137.

[44] J. Mercado, C. Czajkowski, Charged residues in the α [1] and β [2] pre-M1 regions involved in GABA [A] receptor activation, J. Neurosci. 26 (7) (2006) 2031–2040.

[45] J.D. Thompson, D.G. Higgins, T.J. Gibson, CLUSTAL W: improving the sensitivity of progressive multiple sequence alignment through sequence weighting, position-specific gap penalties and weight matrix choice, Nucleic Acids. Res. 22 (22) (1994) 4673–4680, http://www.ebi.ac.uk/clustalw (Online).
[46] A. Bairoch, B. Boeckmann, S. Ferro, E. Gasteiger, Swiss-Prot: juggling between evolution and stability, Brief Bioinform. 5 (1.) (2004) 39–55, http://www.expasy.org/sprot (Online).
[47] Z. Xu, S. Fang, H. Shi, H. Li, Y. Deng, Y. Liao, J.M. Wu, H. Zheng, H. Zhu, H.M. Chen, S.Y. Tsang, H. Xue, Topology characterization of a benzodiazepine-binding beta-rich domain of the GABAA receptor alpha1 subunit, Protein Sci. 14 (10) (2005) 2622–2637.
[48] Q. Huang, X. He, C. Ma, R. Liu, S. Yu, C.A. Dayer, G.R. Wenger, R. McKernan, J.M. Cook, Pharmacophore/receptor models for GABA (A)/BzR subtypes (alpha1beta3gamma2, alpha5beta3gamma2 and alpha6beta3gamma2) via a comprehensive ligand-mapping approach, J. Med. Chem. 43 (1) (2000) 71–95.
[49] T. Nicolas, O.B. Hugues, A. Francine, Are you sure you have a good model? in: T. Langer, R.D. Hofmann (Eds.), Pharmacophore and Pharmacophore searches, Wiley–VCH, Weinheim, Germany, 2006, p. 338.
[50] D.E. Patterson, R.D. Cramer, A.M. Ferguson, R.D. Clark, L.E. Weinberger, Neighborhood behavior: a useful concept for validation of "molecular diversity" descriptors, J. Med. Chem. 39 (16) (1996) 3049–3059.